SISSA

Multimode interferometers for integrated transceivers on 250 nm SOI platform

To c te th s art c e: Y. Zhang *et al* 2020 *JINST* **15** P02022

V ew the art c e on ne for updates and enhancements.

Multimode interferometers for integrated transceivers on 250 nm SOI platform

Y. Zhang,[1] **M. Schneider, L. Eisenblätter, D. Karnick, T. Kühner and M. Weber**

Karlsruhe Institute of Technology, Institute for Data Processing and Electronics,
Hermann-von-Helmholtz-Platz 1, 76344 Eggenstein-Leopoldshafen, Germany

E-mail: zhang.yunlong@partner.kit.edu

ABSTRACT: Multimode interferometers (MMIs) are key components for high-performance transceivers in upgrading the data transmission of future detector systems. According to their power splitting ratio, they are used in Mach-Zehnder modulators and for working point control, respectively. To meet with special requirements, we investigate MMIs with engineered refractive index where sub-wavelength gratings and shallow etching techniques were adopted. By engineering the refractive index of the relevant parts of MMIs, the on-chip footprint and the phase errors can be decreased dramatically, making them suitable for advanced silicon photonic integrated transceivers. These MMIs are compared to two MMIs designed using conventional methods and fabricated on a 250 nm silicon-on-insulator (SOI) platform.

KEYWORDS: Optical detector readout concepts; Data acquisition concepts

---

[1]Corresponding author.

1 Introduction

In 1890, the Talbot effect was observed [1] that if a monochromatic optical plane wave is incident upon a periodic diffraction grating, the grating image will repeat itself at a fixed distance L. The regular distance L is called the Talbot length. This effect was verified by Rayleigh [2] and proved based on Fresnel images in [3]. In addition, secondary imaging at L·p/q was predicted correctly [4] afterwards. With relating the output image to the input source via a convolution, the Talbot effect was extended to two dimensional images [5]. Producing a confined Talbot effect is the basic idea of the MMI and was proposed in [6] and [7] by using total internal reflection in optical fiber to replicate periodic gratings. This phenomenon was firstly tested in 1975 by Ulrich et al. [8]. As MMIs have the merits of compact on-chip footprint, phase-dependent, low loss and predictable performance, they are widely used in photonic integration designs. Additionally, MMIs are also potential structures to optimize the performance of our Echelle grating multiplexers [9].

In the past decade, research interest on MMI forwarded into devices with sub-wavelength structures where the sub-wavelength periodic structures are composed of different materials and helpful to suppress diffraction effects. This diffraction suppression effect became known to researchers was rather early, in the late 19th century [10] whereas the study of electromagnetic wave propagation in a medium, structured at sub-wavelength scale was started rather late in 1940s [11]. In 1950s, Rytov [12] developed a comprehensive theory of sub-wavelength structures. Since then, this topic became more and more popular [13–22]. However, due to limitations of fabrication technology, sub-wavelength structures were not widely used in integrated optics. Recently, with the development of advanced lithography and photonic technologies, they start to be used in integrated circuits design such as grating couplers [23], vertical-cavity surface-emitting lasers [24], and wavelength demultiplexers [25]. In this paper, we present the design of two different types of traditional 2× 2

MMIs with different splitting ratio, the simulation and measurement results of the fabricated devices. Based on these devices we engineer the refractive index of the relevant regions of n × n MMIs to improve their performance accordingly. Appropriate sub-wavelength structures to engineer 2× 2 MMI are simulated and compared to the traditional MMIs.

2   Theory and simulation basics

To calculate the electric field in the waveguide of MMI, the Laplace equation (2.1) has to be solved with considering polarization. In this paper, TE polarization is universally assumed, yielding a problem of solving the one dimensional Helmholtz equation (2.2) where k is the free space wavenumber, n is the refractive index of the core and β is the propagation constant.

$$\nabla^2 \vec{E} + \frac{n^2}{c^2} \vec{E} = 0 \tag{2.1}$$

$$\frac{dE_y^2}{dx^2} + \left(k^2 n^2 - \beta^2\right) E_y = 0 \tag{2.2}$$

$$\beta_0 - \beta_m = \frac{m(m+2)\pi}{3L_c} \tag{2.3}$$

Under the circumstance of strongly guided eigenmodes and paraxial approximation, the propagation constant has the form of $\beta_m = kn\sqrt{1 - \left(\frac{m\pi}{Wkn}\right)^2}$, where W is the width of the multimode region of the MMI. The self-imaging length of the input image is proportional to the beat length $L_c = \frac{\pi}{\Delta\beta_{01}} = \frac{\pi}{\beta_0 - \beta_1}$. In addition, for lower order modes, the quadratic relation meets relation (2.3). If changing the coordinates of the input image, the number and coordinates of the replica images can be dramatically different. A detailed analysis can be found in [26, 27].

Fundamental research on MMI has been investigated widely while the accurate calculation of MMI geometry still cannot be conducted by hand. In this paper, we use commercial software COMSOL Multiphysics to make the numerical simulation. The advantage of the software is that there is an interface with MATLAB via LiveLink™ and one can program complex geometries instead of drawing them one by one in COMSOL. For the sub-wavelength MMIs with many periodic gratings in the following sections, we uniformly programed the geometry in MATLAB and export the device into COMSOL. We use the Wave Optics module and conduct the simulation in frequency domain. All the required materials are included in the library. To obtain accurate result, a small mesh is recommended and the size should be at least 3 times smaller than the effective wavelength. One can also sweep the parameters with any random combination according to their simulation time and computer power.

3   Two conventional MMIs

3.1   3 dB MMIs

The 3 dB-MMIs (also referred to 2× 2 50:50 MMIs in this paper) are key components for the Mach Zehnder modulator (MZM) design [29]. They are used as power splitter and combiner at the two ends of the MZM. There are two alternative schemes to realize the design according to the self-imaging theory where the location of I/O ports and the width of the multimode region are different. We

consider the 250 nm SOI platform, the I/O ports are universally tapered from 0.5 μm over a distance of 10 μm in this paper and we fix the distance between adjacent I/O ports to be 0.5 μm. By sweeping the length of the multimode region and the location of the I/O ports, we obtained two optimized geometries shown in figure 1 and figure 2. The double imaging positon of the MMIs in the two schemes are located at $x = \frac{1}{6}L$ and $x = \frac{1}{2}L$ (with $L = 3L_c$), respectively. It is easy to find that both MMIs have similar on-chip footprint while the one presented in figure 1 has a shorter multimode region and a larger vertical distance between the I/O waveguides and the boundary of multimode region.
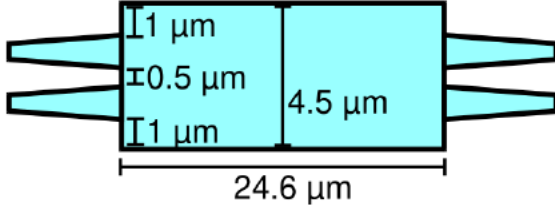
Figure 1. Schematic of first type 3 dB-MMI.
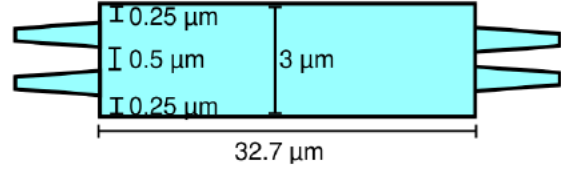
Figure 2. Schematic of a second type of 3-dB MMI.

Hence, we fabricated the MMI shown in figure 1 at IMS Chips (Institut für Mikroelektronik Stuttgart, Germany). For the measurement in this paper, we use a tuneable laser source Agilent 81618A to generate continuous-wave signal where the wavelength can range from 1524 nm to 1576 nm with a depth of 0.5 nm. Between the laser source and the photonic chip, a polarization controller is used to ensure the TE polarization. The output light from the photonic chip will be detected by the embedded detector head of the laser. Limited by the measurement setup, we can merely measure one arm one time. The absolute transmission of MMI arm is derived by subtracting the transmission of the grating couplers from the transmission of the measured MMI arm.

Figure 3 shows the simulated and the measured power fraction of the output power with respect to the input power of two output ports and the inset is a microscope picture of the fabricated device. As can be seen, there is an excellent agreement between the theoretical (dotted lines) and experimental (full lines) results. Across the C band, the input power distributed in two arms is split evenly, the power fraction of both arms remains close to 0.5. Even in the worst case, the power fraction is still as high as 0.45. As a result, the total insertion loss is very low, both the simulation and measurement result are shown in figure 4. The measured average and maximum insertion loss are 0.43 dB and 0.84 dB, respectively.

3.2   2× 2 86:14 MMIs

For working point control using a feedback loop, the awareness of the signal phase is very important in phase modulation. However, detecting the phase of a signal directly is dicult to implement. Since MMIs have a specific phase relation between the I/O ports, we propose utilizing 2× 2 MMIs with an extremely uneven splitting ratio to branch off a certain percentage of the signal in each MZM arm and track their phase relation. According to the MMI self-imaging theory, $x = 1/4\,L$ is also a double imaging position, while the power apportionment is 86:14 instead. More importantly, the phase difference of the two output ports remains 90°. By extensive numerical simulations, we obtained the optimized geometry as the inset picture shows in figure 5. The simulation result show
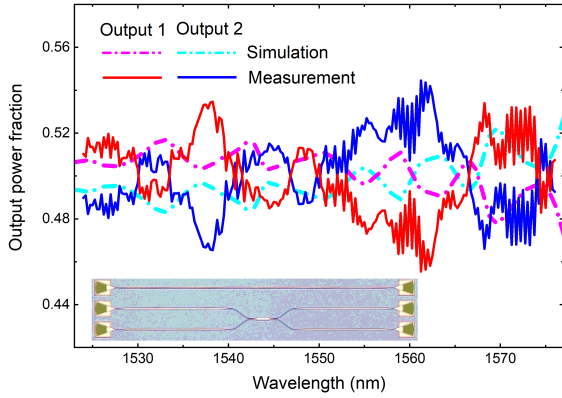
Figure 3. Comparison of simulated and measured power fraction of output ports with respect to the input power of device shown in figure 1.
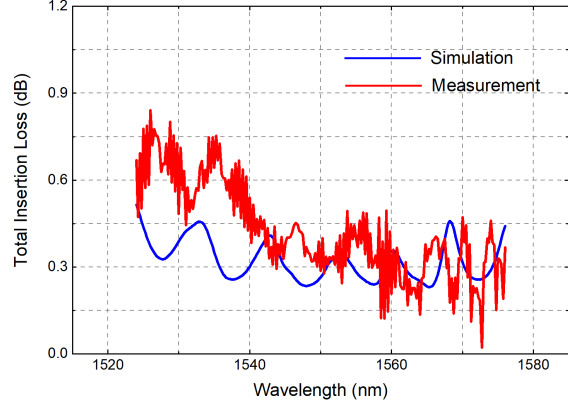
Figure 4. Simulated and measured total insertion loss as a function of wavelength for device shown in figure 1.
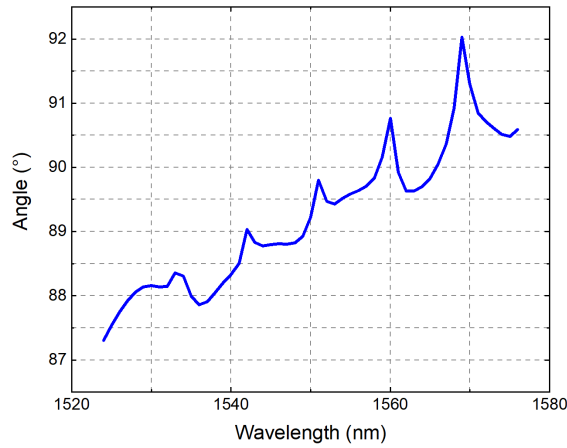
Figure 5. Simulated phase difference of the two output ports of the 2× 2 86:14 MMI. The inset shows the geometry of the MMI.

that the phase difference across the C band is extremely close to the theoretical value, where the average value is 89.2° and the value in the worst case is 87.3°

The simulated and measured power fractions of the designed 2× 2 86:14 MMI are illustrated in figure 6. As can be seen, the power fraction remains very stable and close to the theoretical number throughout the entire C band, resulting in a very low total insertion loss of 0.078 dB in average. It is worth noting, the arm with the major power has an average insertion loss of 0.77 dB given regarding the power in the other arm as insertion loss as well, namely about 86% input power is guided to this port, only 4% power less than in a common 90:10 power splitter. A 90:10 power splitter based on MMIs can only be realized by either adding additional structures (normally a phase shifter) [36] or by combining multiple stages of 3 dB-MMIs, which makes the design large and complex and the fabrication expensive. In comparison, the design proposed in this section is easier to implement, more suitable for integration with slightly less guided power, and finally the exact portion of the branched off signal is not really relevant, as long as it is known and reproducible.
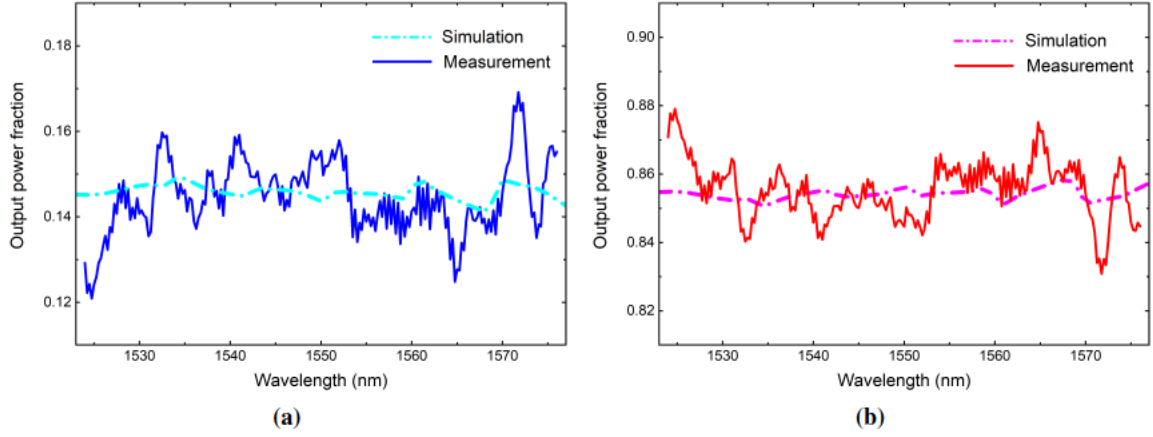
Figure 6. Comparison of simulated and measured power fractions of the output ports with respect to the input power of the 2× 2 86:14 MMI. (a) arm 1 and (b) arm 2.

4 MMIs with engineered refractive index

4.1 A shortened 2× 2 50:50 MMI with sub-wavelength structures

Using sub-wavelength structures is one effective way to construct metamaterials [29, 30], where the optical properties of the metamaterials can be designed according to certain requirements. The sub-wavelength structures have geometries at a scale smaller than the wavelength of the light propagating through. Figure 7 (a) shows an arbitrary 2D dielectric structure. The light propagation layer has alternate regions with refractive indices of n_1 and n_2. The top cladding and bottom substrate layers have refractive indices of n_2 and n_3, respectively. If the pitch size Λ_z is shorter than the shortest Bragg period, the stratified structure behaves as a homogeneous medium with an equivalent refractive index of n_{eq}, as figure 7 (b) shows. The Rytov's formulae [12] are good start to calculate the equivalent refractive index where $n_{\parallel}$ and $n_{\perp}$ in the following relations (4.1) and (4.2) are the directions parallel and perpendicular to the interfaces between the alternating layers, respectively. More accurate result requires numerical calculation.

$$n_{\parallel}^2 = \frac{a}{\Lambda}n_1^2 + \left(1 - \frac{a}{\Lambda}\right)n_2^2 \tag{4.1}$$

$$\frac{1}{n_{\perp}^2} = \frac{a}{\Lambda}\frac{1}{n_1^2} + \left(1 - \frac{a}{\Lambda}\right)\frac{1}{n_2^2} \tag{4.2}$$

For the conventional MMIs, the phase difference between all the guided modes with respect to the phase of the input image at x = 0 is alternatively even and odd multiples of π, and the first inverted replica of the input field appears at x = L. By introducing a small perturbation to modify the modal phase relations, the length to generate the first inverted replica can be shorted dramatically without significantly affecting the mode profiles. In [32] and [33] the authors proposed to use a narrow lengthwise slot at the center of the multimode region, shortening the 2× 2 50:50 MMI by a factor of 2. If the slot is narrow enough, only the propagation constants of even modes are modified whereas those of odd modes are not, since their intensity is zero at the center of the multimode region. As a result, the phase changes of even and odd modes can be modified to be alternatively even and odd

multiples of π at the distance of 0.5L, namely the required length of the first inverted replica of the input field is halved. Therefore, the footprint of MMIs is halved as well. The challenge for this kind of device mentioned in the literature above is that an additional, precisely aligned shallow etching process step is required to introduce phase perturbation.
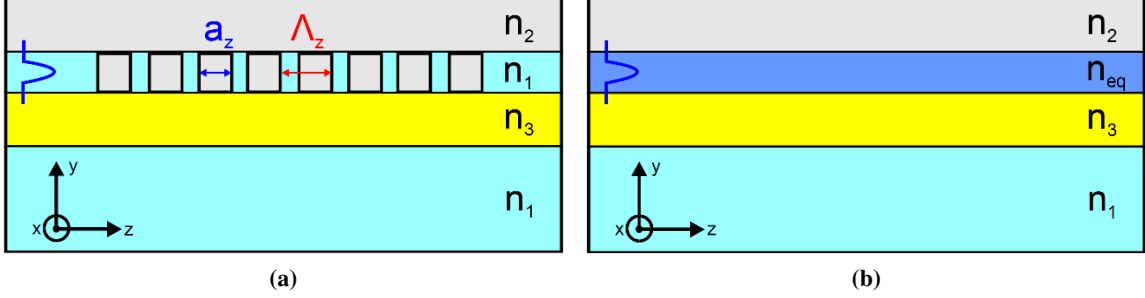
Figure 7. 2D schematic of a slab waveguide with (a) sub-wavelength structures and (b) its equivalent structure with equivalent refractive index.

Alternatively, one can also introduce a small perturbation of refractive index by using sub-wavelength structures. According to the study in [34], for two-material alternating structure, the refractive index in the Bragg reflection region follows a linear relation $n_B \sim \frac{1}{2}(\lambda/\Lambda_z)$ which gives a good starting point to make the calculations of the required modified refractive index of the central region. To obtain a 50:50 splitting ratio with halved length, we made simulations with varying widths and refractive indices of the central engineered region. Figure 8 shows the simulation results at 1550 nm. As can be observed, a narrower width of the central engineered region requires a larger change of the refractive index. Whereas, a width of 60 nm is a limitation for most foundries, in our case, a width of 60 nm and Δn_c = -0.35 is considered. We further made numerical simulations to achieve the engineered Δn_c = -0.35 with a row of SiO2 filled square holes with a lateral length of a = 60 nm and a pitch of Λ = 250 nm. The structure size is well within the fabrication ability of most fabs. Figure 9 shows the simulation results of the designed shortened MMI, the average total insertion loss is as low as 0.21 dB with a maximum value of 0.65 dB at 1480 nm and a minimum value of 0.07 dB at 1565.5 nm. Additionally, the power of the two output ports is almost equal from 1500 nm to 1630 nm with only minor variations. The merits of high bandwidth and compactness make this kind of MMI very suitable for integrated high-bandwidth transceiver designs.

4.2 Low phase error 4× 4 MMIs

The number of guided modes in an MMI is determined by the width of the multimode region. An MMI with multiple ports will result in a wide multimode region and therefore a large number of guided modes. Under the circumstances of numerous guided modes, the parabolic law in (2.3) is not well fulfilled in practice. Therefore, the output images are not perfectly replicated and the guided modes do not interfere with the correct phases. The modal phase error at a distance of N-fold images is approximated by [35]:

$$\Delta\varphi_m \cong m^4 \cdot \frac{\lambda_0^2 \cdot \pi}{2N \cdot n^2 W^2} \cdot \left[\frac{\lambda_0}{6\pi W} \cdot \frac{1}{\left(1 - \Delta n^{-2}\right)^{3/2}} - \frac{1}{8} \right] \tag{4.3}$$
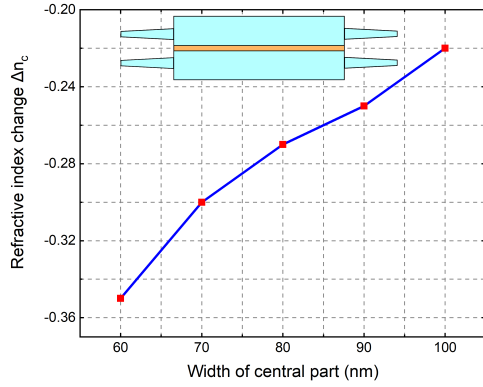
Figure 8. Required refractive index change of the central part with varying width to reduce the length of the MMI by a factor of 2. Inset is the schematic for a 2D structure.
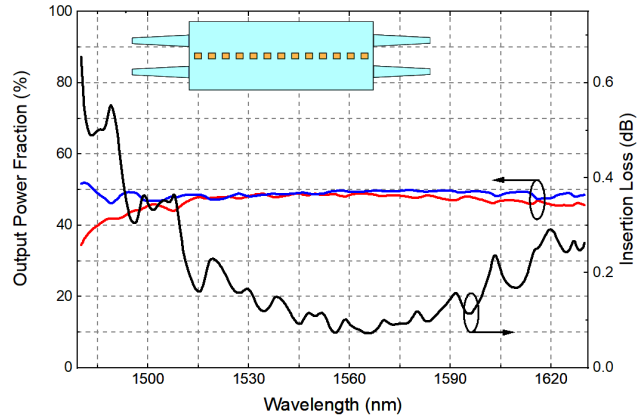
Figure 9. Simulation results of a 3 dB-MMI with sub-wavelength grating in the central part to replace a shallow etched line. Inset is the schematic for the 2D structure.

In this formula, n is the refractive index of the core, Δn is the refractive index contrast ratio between core and lateral cladding, and W is the effective width of the multimode region for the fundamental mode. Two main sources of phase error are the mode number m and the refractive index contrast Δn. Given the mode number m is fixed to a specific value, the phase error will be positive when Δn is small. Conversely, it will be a negative value when the refractive index contrast is high. Considering a 4× 4 MMI on the 250 nm SOI platform, $\Delta n = n_{Silicon}$ - $n_{Silicondioxide}$ is as high as 1.49 ($n_{Silicon}$ = 2.93 and $n_{Silicondioxide}$ = 1.44), the resulting phase error is a negative value and the value for the tenth order will be considerably high according to (4.3). To reduce the phase error, one can optimize the refractive index contrast to an appropriate value. Apart from the phase error, the total insertion loss is also important for MMIs design. Figure 10 shows the simulated total insertion losses of optimized 4 × 4 MMIs at different Δn. When the cladding has a refractive index decrease of 0.3 compared to the core, the total insertion loss is minimum.
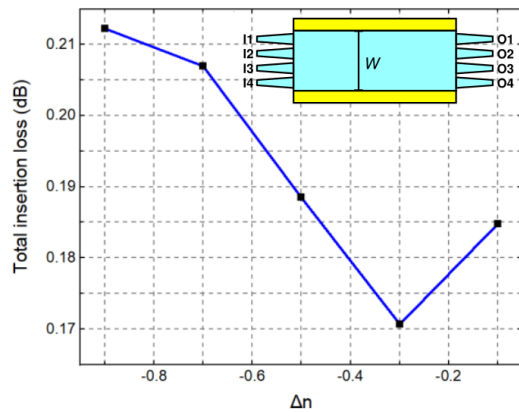
Figure 10. Total insertion loss of optimized 4× 4 MMI over the refractive index change of the lateral cladding with respect to the core. Inset is the 2D structure of 4× 4 MMI.
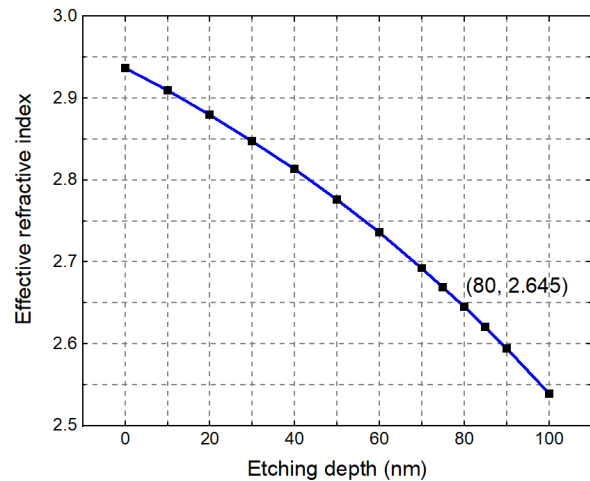
Figure 11. Refractive index engineering effect of different etch depths for the core layer.
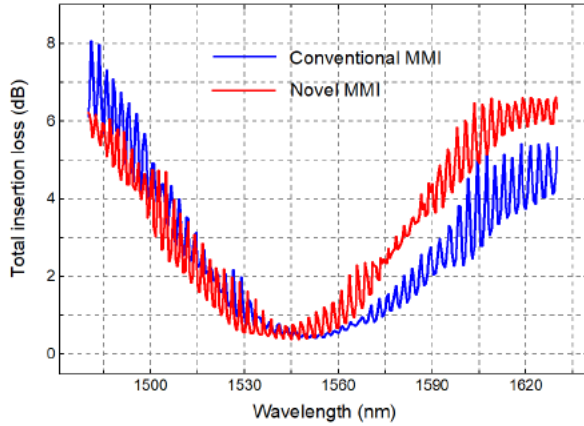
Figure 12. Simulated total insertion loss for conventional and novel 4× 4 MMIs.
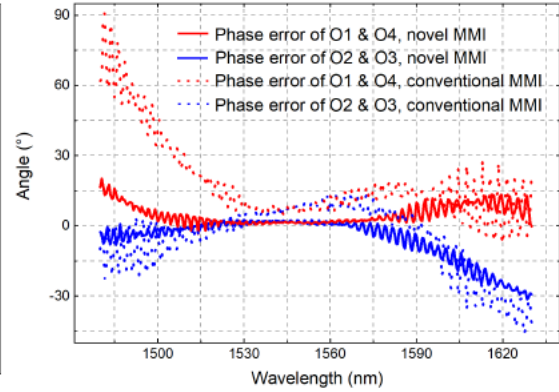
Figure 13. Simulated phase errors between corresponding output ports for conventional and novel 4× 4 MMIs.

There are two options to engineer the refractive index of the lateral cladding region. One solution is using the sub-wavelength gratings similar to those structures shown in section 3.1. The advantage of this method is that no additional etching steps are required. However, to get accurate numerical simulation results using commercial software is extremely computing source consuming for such a large device with numerous sub-wavelength structures. In this case, using a shallow etched region is the favourable solution. A calculation of the effective refractive index for different core layer thicknesses was made and the result is shown in figure 11. As can be seen, an etch depth of 80 nm will result in an effective refractive index of 2.645, where the refractive index difference to an non-etched core layer is close to 0.3. With this configuration, the final optimized 4× 4 MMI has an on-chip footprint of 7.2 μm × 105.6 μm. Figure 12 and figure 13 show the simulated total insertion loss and the phase errors, respectively. The novel MMI has a bandwidth of approximately 80 nm, which is comparable to the conventional MMIs. Whereas, the maximum phase error in the C band for the novel MMI is merely 3.1°, much smaller than the 10.3° of conventional MMI.

5 Conclusions and outlook

In this paper, several different types of MMIs were presented. The fabricated 3-dB MMI has a compact geometry of 4.5 μm × 24.6 μm on a 250 nm SOI platform. A second MMI with a power splitting ratio of 86:14 has a more compact geometry of 2.8 μm × 14.2 μm. Both devices show excellent agreement with simulation results and the splitting ratio remains stable across the C-band. Additionally, they feature a low insertion loss with an average value of less than 0.8 dB. The performance of MMIs can be further improved by engineering the refractive index of certain parts. By introducing sub-wavelength grating elements with a size of 60 nm × 60 nm, the size of a 3 dB-MMIs can be halved without deteriorating the performance. By lowering the refractive index contrast between the core and lateral cladding of 4× 4 MMIs, the maximum phase error can be decreased from 10.3° to 3.1°. We propose to implement the engineered refractive index by an etching depth of 80 nm and the resulting MMI has an on-chip geometry of 7.2 μm × 105.6 μm. These results will contribute to an improved performance of higher integrated high-bandwidth transceivers.

Acknowledgments

References

[1] H. Talbot, *LXXVI. Facts relating to optical science. no. IV*, *London Edinburgh Dublin Phil. Mag. J. Sci.* **9** (1836) 401.

[2] L. Rayleigh, *XXV. On copying diffraction-gratings, and on some phenomena connected therewith*, *London Edinburgh Dublin Phil. Mag. J. Sci.* **11** (1881) 196.

[3] J.M. Cowley and A.F. Moodie, *Fourier images: I — the point source*, *Proc. Phys. Soc.* **B 70** (1957) 486.

[4] E.A. Hiedemann and M.A. Breazeale, *Secondary interference in the Fresnel zone of gratings*, *J. Opt. Soc. Amer.* **49** (1959) 372.

[5] J.T. Winthrop and C.R. Worthington, *Theory of Fresnel images I plane periodic objects in monochromatic light*, *J. Opt. Soc. Amer.* **55** (1965) 373.

[6] L.A. Rivlin and V.S. Shul'dyaev, *Multimode waveguides for coherent light*, *Radiophys. Quant. Electron.* **11** (1968) 318.

[7] O. Bryngdahl, *Image formation using self-imaging techniques*, *J. Opt. Soc. Amer.* **63** (1973) 416.

[8] R. Ulrich and G. Ankele, *Self-imaging in homogeneous planar optical waveguides*, *Appl. Phys. Lett.* **27** (1975) 337.

[9] Y. Zhang et al., *Low-loss and robust DWDM Echelle grating (de-)multiplexers in SOI technology*, *Proc. SPIE* **10914** (2019) 109140J.

[10] H. Hertz, *Ueber Strahlen electrischer Kraft* (in German), *Annalen Phys.* **272** (1889) 769.

[11] I.E. Tamm and V.L. Ginzburg, *Theory of electromagnetic processes in a layered core*, *Izv. Akad. Nauk SSSR Ser. Fiz.* **7** (1943) 30.

[12] S. Rytov, *Electromagnetic properties of a finely stratified medium*, *Sov. Phys. JETP* **2** (1956) 466.

[13] C.G. Bernhard and W.H. Miller, *A corneal nipple pattern in insect compound eyes*, *Acta Phys. Scandinavica* **56** (1962) 385.

[14] P.B. Clapham and M.C. Hutley, *Reduction of lens reflexion by the "moth eye" principle*, *Nature* **244** (1973) 281.

[15] J.N. Mait and D.W. Prather, *Selected papers on subwavelength diffractive optics*, SPIE Milestone Series, volume MS166, (2001).

[16] P. Yeh, *A new optical model for wire grid polarizers*, *Opt. Commun.* **26** (1978) 289.

[17] E.B. Grann, M.G. Moharam and D.A. Pommet, *Artificial uniaxial and biaxial dielectrics with use of two-dimensional subwavelength binary gratings*, *J. Opt. Soc. Amer.* **A 11** (1994) 2695.

[18] S. Wilson and M. Hutley, *The optical properties of 'moth eye' antireflection surfaces*, *Optica Acta: Int. J. Opt.* **29** (1982) 993.

[19] R.C. Enger and S.K. Case, *Optical elements with ultrahigh spatial-frequency surface corrugations*, *Appl. Opt.* **22** (1983) 3220.

[20] M.E. Motamedi, W.H. Southwell and W.J. Gunning, *Antireflection surfaces in silicon using binary optics technology*, *Appl. Opt.* **31** (1992) 4371.

[21] J.P. van der Ziel, *Phase-matched harmonic generation in a laminar structure with wave propagation in the plane of the layers*, *Appl. Phys. Lett.* **26** (1975) 60.

[22] A. Fiore, V. Berger, E. Rosencher, P. Bravetti and J. Nagle, *Phase matching using an isotropic nonlinear optical material*, *Nature* **391** (1998) 463.

[23] R. Halir et al., *Waveguide grating coupler with subwavelength microstructures*, *Opt. Lett.* **34** (2009) 1408.

[24] M.C. Huang, Y. Zhou and C.J. Chang-Hasnain, *A surface-emitting laser incorporating a high-index-contrast subwavelength grating*, *Nature Photonics* **1** (2007) 119 [*Erratum ibid.* **1** (2007) 297].

[25] P. Cheben et al., *Refractive index engineering with subwavelength gratings for efficient microphotonic couplers and planar waveguide multiplexers*, *Opt. Lett.* **35** (2010) 2526.

[26] M. Bachmann, P.A. Besse and H. Melchior, *General self-imaging properties in* $N \times N$ *multimode interference couplers including phase relations*, *Appl. Opt.* **33** (1994) 3905.

[27] K. Cooney and F.H. Peters, *Analysis of multimode interferometers*, *Opt. Expr.* **24** (2016) 22481.

[28] Y. Zhang et al., *Key building blocks of a silicon photonic integrated transmitter for future detector instrumentation*, 2019 *JINST* **14** P08021.

[29] P. Cheben et al., *Refractive index engineering with subwavelength gratings for efficient microphotonic couplers and planar waveguide multiplexers*, *Opt. Lett.* **35** (2010) 2526.

[30] I. Staude and J. Schilling, *Metamaterial-inspired silicon nanophotonics*, *Nature Photonics* **11** (2017) 274.

[31] L. Soldano and E. Pennings, *Optical multi-mode interference devices based on self-imaging: principles and applications*, *J. Lightwave Technol.* **13** (1995) 615.

[32] J.C. Campbell and T. Li, *Electro-optic multimode waveguide modulator or switch*, *J. Appl. Phys.* **50** (1979) 6149.

[33] D.M. Mackie and A.W. Lee, *Slotted multimode-interference devices*, *Appl. Opt.* **43** (2004) 6609.

[34] P. Yeh, A. Yariv and C.-S. Hong, *Electromagnetic propagation in periodic stratified media. I. General theory*, *J. Opt. Soc. Amer.* **67** (1977) 423.

[35] J. Huang, R. Scarmozzino and R. Osgood, *A new design approach to large input/output number multimode interference couplers and its application to low-crosstalk WDM routers*, *IEEE Photon. Technol. Lett.* **10** (1998) 1292.

[36] F. Ren, W. Chen, T. Zhangsun, Y. Zhang, X. Fan and J. Wang, *Variable-ratio mode-insensitive* 1×2 *power splitter based on MMI couplers and phase shifters*, *IEEE Photon. J.* **10** (2018) 1.